Mine Water Environ (2017) 36:508–519
DOI 10.1007/s10230-017-0438-4

TECHNICAL ARTICLE

Numerical Analysis of Karst Water Inrush and a Criterion for Establishing the Width of Water-resistant Rock Pillars

Yanlin Zhao[1,2] · Shilin Luo[1] · Yixian Wang[3] · Weijun Wang[1] · Lianyang Zhang[4] · Wen Wan[1]

Received: 9 June 2016 / Accepted: 18 January 2017 / Published online: 25 February 2017

Abstract Water-bearing caves in the Maokou limestone have caused disastrous water inrushes in mines in southern China. A linkage analysis between the hydro-mechanical coupling and the strength reduction method was used to investigate the stability of water-resistant rock pillars. The factor of safety (FOS) of the pillar was established, and a criterion for establishing the required width of the pillar was proposed in engineering practice, i.e., the width of the pillar should be based on the blast hole depth and blast-disturbance depth, along with a FOS of 1.5. The permeability of the water-resistant pillar and the probability of water inrush both increase as the strength reduction factor increases because the effective width of the pillar narrows. A numerical analysis of the Qiyi coal mine "4·16" water inrush accident shows that the cause of the inrush was that the 3.0 m wide barrier left by roadway excavation was too narrow to withhold the karst water pressure of about 4.0 MPa.

Keywords Mining engineering · Hydro-mechanical coupling · Strength reduction method · Factor of safety

Introduction

There have been thousands of casualties in groundwater-related coalmine accidents in China since 2000 (Wang et al. 2010; Wu et al. 2004; Wu and Wang 2006; Zhang 2005). Geological settings and hydrogeological conditions of the coalfields are very complicated in southern China, where the main minable coal layer lies in the late Permian Longtan Formation, and a karstic limestone aquifer lies below, in the late Permian Maokou Formation (Dai et al. 2005; He et al. 2011, 2012; Miao et al. 2009; Sun et al. 2012). Due to the inhomogeneity of caves in the Maokou limestone strata, developmental roadways can often be safely constructed in the Maokou limestone, but if water-bearing caves are encountered, karst water may burst through catastrophically, such as the "12.12" accident in 2004 (36 dead), the "9.28" accident in 2010, the "4·16" accident in 2013 (17 dead), and the "6.15" accident in 2014 (9 dead).

A number of empirical criteria and analytical models have been proposed for the analysis and predication of water inrush from underlying confined aquifers, including the: water inrush index; hypothesis of three zones in floor strata; plate model; and key strata model (Xiao et al. 1991; Miao et al. 2011; Shi and Singh 2001; Wang and Park 2003; Zhang 2005). These theoretical investigations have been actively used in evaluating the risk of water inrush hazards.

Electronic supplementary material The online version of this article (doi:10.1007/s10230-017-0438-4) contains supplementary material, which is available to authorized users.

✉ Yanlin Zhao
yanlin_8@163.com

✉ Yixian Wang
wangyixian2012@hfut.edu.cn

[1] Hunan Provincial Key Laboratory of Safe Mining Techniques of Coal Mines, Work Safety Key Lab on Prevention and Control of Gas and Roof Disasters for Southern Coal Mines, Hunan University of Science and Technology, Xiangtan, Hunan 411201, China

[2] State Key Laboratory of Coal Resources and Safety Mining, China University of Mining and Technology, Xuzhou 221008, China

[3] School of Civil Engineering, Hefei University of Technology, Hefei 230009, China

[4] Department of Civil Engineering and Engineering Mechanics, University of Arizona, Tucson, AZ 85721, USA

For a better understanding of water inrush mechanism and process, numerous numerical simulations of water inrush associated with mining process have also been performed (Guo et al. 2009; Jing 2003; Lu and Wang 2015; Zhang et al. 2009; Zhu et al. 2013). For example, Guo et al. (2009) proposed a coupled double porosity FEM code called COSFLOW to predict water inflows. Zhu et al. (2013) presented a coupled numerical model to analyze pore pressure changes during mining. Lu and Wang (2015) presented a micromechanics-based coupled damage and flow modeling approach to simulate progressive development of fractures and the associated water inrush in the floor strata during mining above a confined aquifer. These numerical investigations have shown that permeability coefficient enhancement induced by mining is the key mechanism promoting water inrushes. However, these models did not address the safety requirements of water-resistant rock pillars.

The strength reduction method (SRM), which is based on numerical methods, has been widely applied in slope stability analyses, such as in the studies of Cheng et al. (2007); Dawson et al. (1999); Griffiths and Lane (1999); Lin et al. (2010) and Zienkiewicz et al. (1975). In the SRM, the factor of safety (FOS) is defined as the ratio between the actual shear strength and the reduced shear strength at failure. The effective material strength parameters are reduced until the slope fails, and the corresponding strength reduction factor (SRF) is the FOS of the slope. Some attempts have been made to apply the SRM beyond slope engineering to the stability of other engineering structures, such as in mining engineering and tunnel engineering (Yang and Huang 2009; Yu and Liu 2015; Zhao et al. 2010). However, there has been no reasonable and reliable criterion to assess the FOS of a water-resistant rock pillar based on the SRM.

The rock between the excavation and a water-bearing cave acts as a geological barrier that prevents karst water from entering the roadway. The effectiveness of the geological barrier depends on its width, lithology, and integrity. Water inrush is likely to occur when the barrier is too thin and/or fractured to withhold the pressure of karst water. The stability of a water-resistant rock pillar and its safe width is of great significance for controlling karst water inrush in mine. In this paper, a linkage analysis method (HM-SRM) between the hydro-mechanical coupling (HM) and the strength reduction method (SRM), is proposed to study the stability of the water-resistant rock pillar. A FOS for the rock pillar is established, and a practical engineering criterion is proposed for establishing the pillar width.

Principles of Linkage Analysis between HM and SRM (HM-SRM)

When water-bearing karst features are near a constructed void space, the stress in the surrounding rock, especially in the pillar, will change remarkably, due to the disturbance stress induced by the excavated opening and the water pressure.

Governing Equations of Hydro-mechanical Coupling (HM)

As for the coupling analysis, a coupled hydro-mechanical model was incorporated into the FLAC^{3D} code. The coupling formulation model was based on the following basic assumptions, as summarized from general observations (Cundall 2001; Tang 1997; Yang et al. 2004):

1. The rock mass is fully saturated.
2. The fluid flow conforms to the Biot consolidation theory.
3. The permeability coefficient varies as a function of the stress state in the elastic deformation stage and increases dramatically when the element is in a plastic yielding state (Tang 1997; Yang et al. 2004).

There are three basic equations of the proposed HM model:

1. Seepage equation (Itasca Consulting Group Inc 2002)

The fluid transport is described by Darcy's law, given in the form:

$$q_i = -k_{il}(\Theta, p)\left(p - \rho_w x_j g_j\right)_{,l}, \tag{1}$$

where q_i is the specific discharge vector, $k_{il}(\Theta, p)$ is the permeability coefficient of the rock mass, which is dependent on the stress state and pore pressure, p is water pressure, ρ_w is water density, and g_i, $i=1, 2, 3$ are the three components of the gravity vector.

The fluid mass balance may be expressed as

$$-q_{i,i} + q_v = \frac{\partial \zeta}{\partial t}, \tag{2}$$

where q_v is the volumetric fluid source intensity in, and ζ represents changes in the fluid content. The response equation for the pore fluid in saturated rock masses is formulated as

$$\frac{1}{M}\frac{\partial p}{\partial t} = \frac{\partial \zeta}{\partial t} - \alpha \frac{\varepsilon_v}{\partial t}, \tag{3}$$

where M is the Biot module, α is Biot coefficient, ε_v is the mechanical volumetric strain, and t is fluid flow time.

2. Mechanical equations (Itasca Consulting Group Inc 2002)

Balance equation:

$$\sigma_{ij,j} + f_i = 0 \ (i,j = 1,2,3), \tag{4}$$

where σ_{ij} is the total stress in the *ij*-plane, and f_i is the body force.

Compatibility equation:

$$\varepsilon_{ij} = \frac{1}{2}\left(u_{i,j} + u_{j,i}\right), \tag{5}$$

where ε_{ij} is the strain, $u_{i,j}$ is the displacement in the *i*th direction, and $u_{j,i}$ is the displacement in the *j*th direction.

The constitutive response for rock mass in hydro-mechanical coupling follows the form:

$$\sigma_{ij} + \alpha\frac{\partial p}{\partial t}\delta_{ij} = H\left(\sigma_{ij}, \xi_{ij}\right), \tag{6}$$

where σ_{ij} is the co-rotational stress rate, H is the function form of constitutive law, δ_{ij} is the Kronecker delta, and ξ_{ij} is the strain rate (Itasca Consulting Group Inc 2002).

The Mohr–Coulomb Criterion was used to define the yield criterion, in which the shear failure criteria is:

$$f^s = \sigma_1' - \sigma_3'\frac{1+\sin\phi}{1-\sin\phi} + 2c\sqrt{\frac{1+\sin\phi}{1-\sin\phi}}, \tag{7}$$

and the ensile failure criterion is:

$$f^t = \sigma_t - \sigma_3' = 0, \tag{8}$$

where σ_1' is the first effective principal stress, σ_3' is the third effective principal stress, ϕ is the friction angle of the rock mass, c is cohesion, and σ_t is tensile strength.

3. Permeability coefficient equation

In the HM model, the rock permeability coefficient is decreased or increased as stress changes. The stress-dependent permeability coefficient can be represented as (Li et al. 2011; Yang et al. 2007):

$$k_{il}(\Theta, p) = \xi k_0 e^{-\lambda(\Theta/3-\eta p)}, \tag{9}$$

where k_0 is the permeability coefficient at zero effective stress state i.e. $\Theta/3-\eta p=0$, $\Theta = \sigma_1 + \sigma_2 + \sigma_3$ is the volumetric stress, λ and η are fitting parameters, respectively, ξ is the adjustment coefficient for the plastic yielding element, and λ, η and ξcan be determined by permeability tests on rock specimens in a complete stress–strain process.

In coupling analysis for a rock element in the elastic state, the permeability coefficient is assumed to be a negative exponential function of the volumetric stress (David et al. 2001; Louis 1974). The $\xi = 1.0$ in Eq. (9) and λ as a fitting parameter can be obtained from permeability tests. The permeability coefficient is greatly enhanced when a rock element is in a plastic yielding state, and ξ can be determined by permeability tests on rocks in a complete stress–strain process (Li et al. 1994; Yang et al. 2007).

According to Eq. (9), the permeability coefficient of each element can be grasped by using the FLAC^{3D} programming language (Itasca Consulting Group Inc 2002), and by modifying the permeability coefficient in the seepage constitutive model [Eqs. (1) and (3)] in FLAC^{3D}. When elastic–plastic analysis indicates non-convergence, the water-resistant pillar is unstable and a water inrush is likely.

It should be noted that the permeability coefficient used in FLAC^{3D} is different from the conventional permeability coefficient. The conversion between them is as follows:

$$k_c(\Theta, p) = k_{il}(\Theta, p)\rho_w g = 9.8 \times 10^3 k_{il}(\Theta, p), \tag{10}$$

where k_{il} (Θ, p), as shown in Eqs. (1) and (9), is the permeability coefficient used in FLAC^{3D}, m^2/(Pa s) in SI units, k_c (Θ, p) is the conventional permeability coefficient, m/s in SI units, and g is the gravitational acceleration. To simplify the calculation, the permeability coefficient mentioned below has been converted to a conventional permeability coefficient.

Starting from a state of mechanical equilibrium, a coupled hydro-mechanical static simulation in FLAC^{3D} involves a series of steps. Each step includes one or more flow steps (flow loop) followed by enough mechanical steps (mechanical loop) to maintain a quasi-static equilibrium.

Strength Reduction Method (SRM)

The strength reduction principle is that when actual shear strength parameters: cohesion, c, and friction angle, φ, of the water-resistant rock pillar are divided by the SRF, a new group of shear strength parameters c' and φ' are obtained, which serve as new calculated parameters (Matsui and San 1992).

$$c' = \frac{c}{F_i}, \tag{11}$$

$$\varphi' = \arctan(\tan\varphi/F_i). \tag{12}$$

As the SRF increases, the corresponding calculated parameters c' and φ' are gradually decreased until numerical non-convergence occurs. At that time, the SRF is the FOS of the water-resistant pillar. The convergence criterion in FLAC^{3D} is the nodal unbalanced force ratio, R, required to bring the model to a state of equilibrium, which was set to 1×10^{-5} (per Itasca Consulting Group Inc 2002).

Analysis Procedures of the HM-SRM Method

In the proposed HM-SRM method, the occurrence of water inrush is linked with the non-convergence of the mechanical

calculation, and the seepage characteristics are closely related to the stress state and plastic failure zone. The steps for implementing HM-SRM method in FLAC^{3D} are as follows:

Step 1: Build the calculated model according to geometry, mechanical, and seepage properties of the rock masses, karst water pressure, and boundary conditions; Step 2: Carry out the hydro-mechanical coupling analysis using the Mohr–Coulomb yield criterion, and modify the permeability coefficient of each element according to Eq. (9) to determine the stress and seepage fields; Step 3: Check whether the numerical calculation is convergent or not; Step 4: If the numerical calculation is convergent, the reduced $c^{'}$ and $\varphi^{'}$ are adopted in hydro-mechanical coupling analysis to determine the new stress and seepage fields [Eqs. (11) and (12)]; Step 5: Repeat steps 2–4, and a new SRF is generated until numerical non-convergence occurs; Step 6: The FOS of a given water-resistant rock pillar is equal to the SRF at which numerical non-convergence occurs.

The flow chart for implementing the HM-SRM method is provided as a supplemental file (Appendix 1), which accompanies the on-line version of this paper.

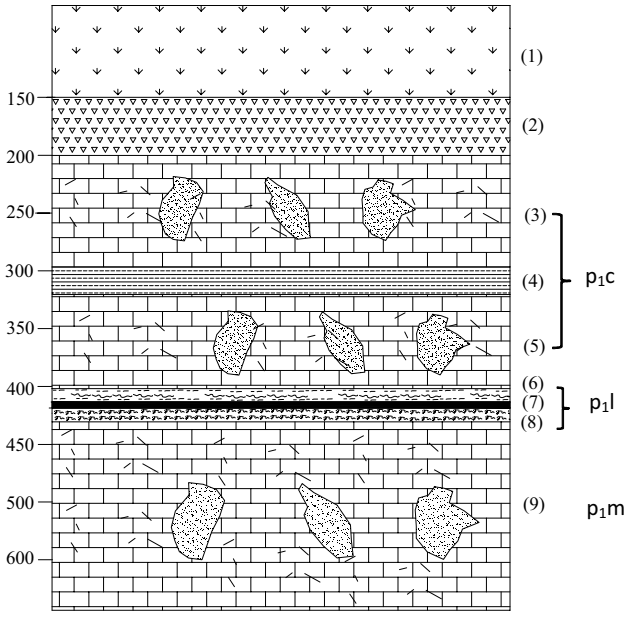

Fig. 1 The geologic profile: (*1*) Quaternary strata, (*2*) Cretaceous strata, (*3*) Limestone 10#, (*4*) Mudstone, (*5*) Limestone 11#, (*6*) Mudstone, (*7*) Coal seam, (*8*) Sandstone, and (*9*) Limestone #12

Case Analysis

Water Inrush Accident

The HM-SRM method was used to evaluate the safety margin of the water-resistant pillar and the process of karst water inrush in the Qiyi coal mine, in Hunan province, in southern China. The geologic profile comprises Quaternary, Cretaceous, and Permian strata (Fig. 1). The Permian System is divided into three formations, the: Changxin Formation (p_1c), with an average thickness of 200 m; Langtan Formation (p_1l), with an average thickness of 27.4 m; and Maokou Formation (p_1m), which is about 300 m in thickness. The p_1c Formation is composed dominantly of dark and medium gray layers of bituminous limestone and mudstone. The p_1c Formation is the major coal-bearing formation and consists of sandstone, mudstone, and the #2 coal seam, with an average thickness of 3.75 m. The P_1m Formation consists mainly of grayish-white thick-layered calcareous limestone. Caves, grikes, and erosion cracks are developed in the p_1c and p_1m Formations.

The heading face at the −160 m level in the No. 23 mining area was located in the Maokou limestone strata. On 16 April 2013, 17 people died when a huge water inrush occurred at the heading face. At 8 am, karst water burst suddenly through the face, approximately 1 h after the blasting and the mucking process. The initial inflow was estimated at 3,670 m^3/h. After about 2 h, the water level had risen by as much as 2.5 m, and about 2 km of the roadway was flooded. About 22, 500 m^3 water in total burst out within nearly 11 h. A cave with a volume of about 20 m×6 m×20 m was exposed about 3 m in front of the heading face after the damage was cleared. The geological survey indicated that there were major fractures and well-developed caves around the roadway where the water inrush took place. The depth of the roadway excavation was about 430 m, the hydrostatic pressure head was about 400 m, and the water pressure in the cave was about 4.0 MPa. A spot investigation found that the surrounding rock was largely dissolved, and the water could have been supplied by karst pathways.

Determination of Mechanical and Hydraulic Properties

To obtain the mechanical and hydraulic properties of the fractured Maokou limestone for the numerical model, a series of laboratory tests were performed on fractured limestone specimens from the surrounding rock at the water inrush location. For more detail on these tests, see "Appendix 2" in the online version of this paper. Based on these experimental data, the parameters related to the mechanical and hydraulic properties of the fractured limestone are listed in Table 1. Based on the permeability tests in the complete stress–strain process, the parameter λ in Eq. (9) was set to 0.6, the k_0 of 7.84×10^{-10} m/s was converted to a conventional permeability coefficient, and λ was 0.0822. The adjustment coefficient$\zeta$for the plastic yielding elements is 105 (Zhao et al. 2017).

Calculation Model

The numerical model was established based on the in situ conditions at the Qiyi Coal Mine. The simulation domain was 50 m in length, 20 m in width, and 30 m in depth (Fig. 2a), and the excavated roadway had a semi-circular arched cross-Sect. (2.5 m in width and 3.2 m in height), which was situated in the middle of the model (Fig. 2b). The water-bearing cave is on the right edge of the model, and was simplified as an ellipsoidal shape with a long axis of 20.0 m and a short axis of 6.0 m.

The four boundaries, except for the bottom and top boundaries, were allowed to move vertically but were horizontally restrained. The bottom of the model was fixed in terms of depth. At the top of the model, a vertical load (σ_1 = 10 MPa) was applied to simulate the overburden weight. The boundary condition of the seepage field was as follows: the karst water pressure was assumed to be 1.0, 2.0, 3.0, 4.0, and 5.0 MPa, respectively, to simulate various artesian pressures. The numbers 1 through 5 in Fig. 2a simulates steps in the excavation, with every step in the numerical simulation set at 5.0 m if the width of the water-resistant pillar between the excavated opening and the cave was larger than 10.0 m, and at 2.5 m if the width of the water-resistant rock pillar was less than 10.0 m, so that the stability of the water-resistant rock pillar could be studied with different width values.

For the convenience of the research, an example was set up with the HM-SRM method used to investigate the stability of an 8.0 m wide water-resistant pillar subjected to an assumed karst water pressure of 4.0 MPa.

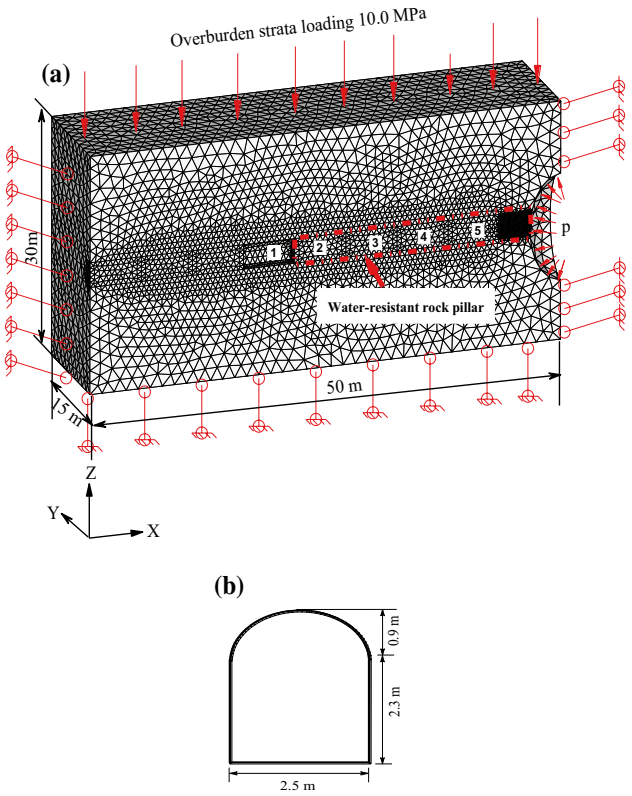

Fig. 2 Numerical analysis model of karst water inrush: **a** loading and boundary conditions; **b** the size of the heading face

Mechanical Analysis of Rock Pillars with Various SRFs

Figures 3, 4 and 5 represent the vertical stress distribution in a water-resistant pillar with SRFs of 1.10, 1.54, and 1.59. During the excavation stage, mechanical changes develop in the water-resistant pillar due to stress redistribution around the newly excavated opening and the hydraulic pressure gradient applied onto the pillar.

When the SRF was 1.10, the vertical stress was concentrated and formed a pressurized area in the rock between the excavated area and the cave (Fig. 3a). The plastic zone was mostly distributed near the excavation and the cave (Fig. 3b). The vertical stress distribution in the plastic zone gradually rose from the excavated area or the cave towards the interface of the plastic and elastic zones. In the elastic zone, the vertical stress gradually decreased from the peak stress on the interface of the elastic and plastic zones to the original rock stress. The width of the plastic zone extended about 2.0 and 1.1 m into the rock pillar from the excavation and cave, respectively, and the width of the elastic zone was about 4.9 m at an SRF of 1.10. With an increased SRF, the average vertical stress shrinks, the range of the plastic zone is broadened, and the pressurized zone moves toward the middle of the rock pillar. For example, when SRF = 1.54, the average vertical stress was 72.5% of what it was at SRF = 1.10 (Fig. 4a), the plastic zone broadened, and the elastic zone narrowed to a band =0 m in width (Fig. 4b).

Table 1 Parameters related to mechanical and hydraulic properties of the fractured limestone

Density (g/cm^3)	Elastic modulus (GPa)	UCS (MPa)	Tensile strength (MPa)	Poisson's ratio	Friction angle (^{o})	Cohesion (MPa)	Initial permeability coefficient (10^{-10}m/s)	Porosity
2.51	10.6	20.8	1.81	0.232	29.5	1.50	4.20	0.162

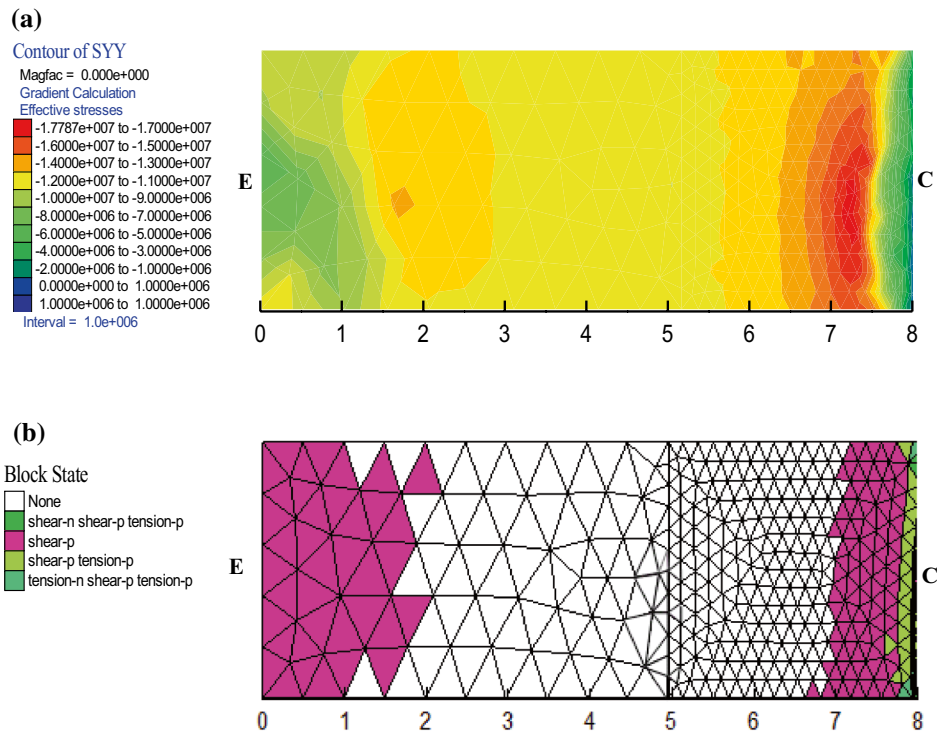

Fig. 3 **a** Vertical stress distribution, and **b** plastic zone in a water-resistant rock pillar at a SRF of 1.10. The E side is the excavated opening, and the C side is the water-bearing cave

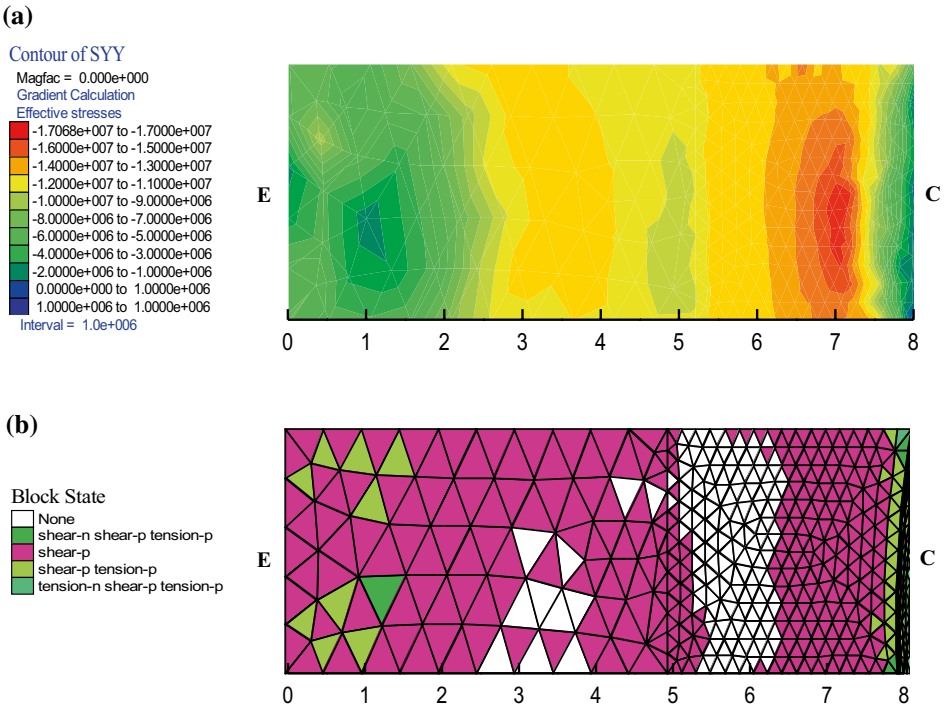

Fig. 4 **a** Vertical stress distribution, and **b** plastic zone in a water-resistant rock pillar at a SRF of 1.54. The E side is the excavated opening, and the C side is the water-bearing cave

When SRF = 1.59, most of the water-resistant pillar was in a plastic state, with a numerical non-convergence (Fig. 5b). Since the calculated result failed to converge to a steady value at SRF = 1.59, at calculation step N = 6,000 for example, the vertical stress distributed in the pillar is mostly in a range from −2.0 MPa to −6.0 MPa; local tensile stress occurs near the excavated opening at calculation step N = 6000 (Fig. 5a). The plastic zone in the pillar nonlinearly increased as the SRF increased (Fig. 6). For example, the proportion increased from 38.2 to 77.6% as

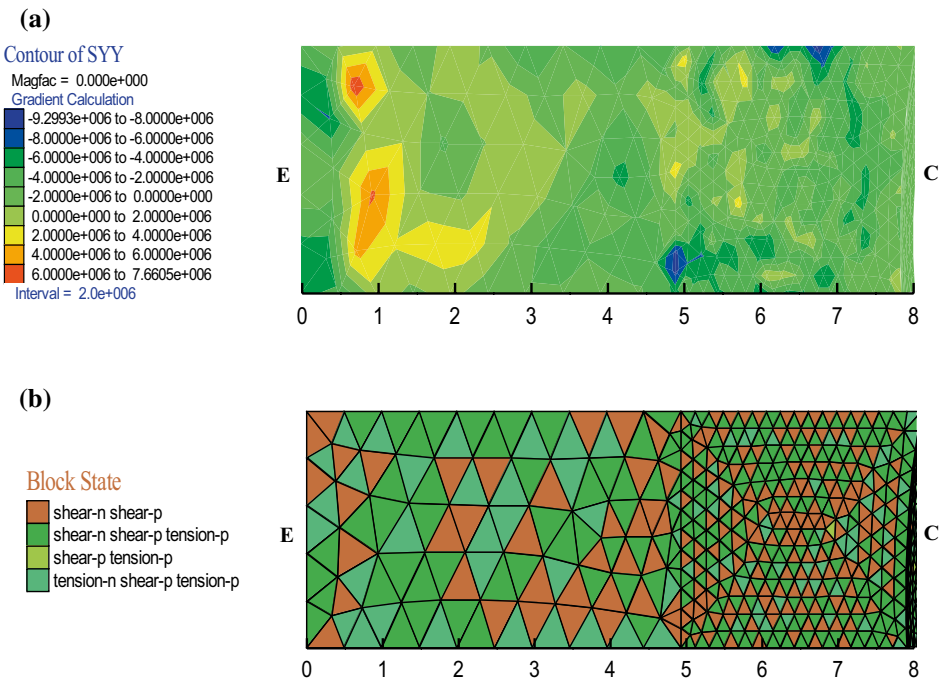

Fig. 5 **a** Vertical stress distribution, and **b** plastic zone in a water-resistant rock pillar at a SRF of 1.59. The E side is the excavated opening, and the C side is the water-bearing cave

the SRF increased from 1.10 to 1.54. At an SRF of 1.59, almost the entire rock pillar was in a plastic state, which means the pillar was unstable. So the FOS of the water-resistant rock pillar was 1.59 at a pillar width of 8 m and a karst cave water pressure of 4.0 MPa. It should be noted that although numerical non-convergence occurs as the pillar loses stability, the other zones in the calculation model remain stable.

In fact, the effective width of the pillar is the width of its elastic zone, which is far less than its physical width, because the plastic zone is ineffective in preventing karst water inrush. As the SRF increases, the elastic zone in the rock pillar narrows, while the plastic zone broadens, which means that the effective width of the water-resistant pillar decreases and the probability of water inrush increases. The discharge in the excavated opening increases in conformity with the development of the plastic zone in the pillar. Both increase gradually at SRFs of 1.10–1.50, but increase sharply at SRFs above 1.50, synchronously, until numerical non-convergence occurs at an SRF of 1.59 (Fig. 6).

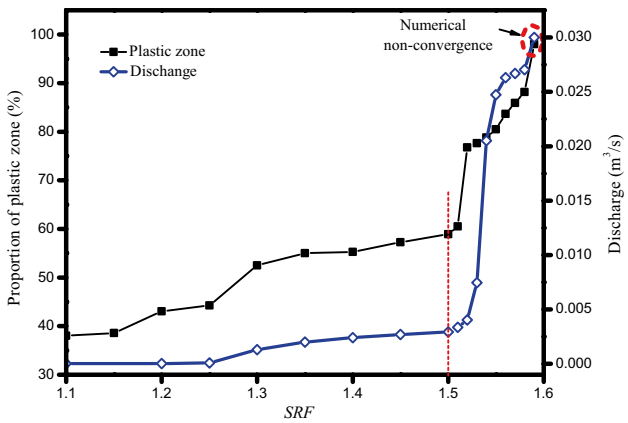

Fig. 6 Proportion of the plastic zone in the rock pillar, and the discharge of the excavated opening versus *SRF*

Permeability of the Water-resistant Rock Pillar with Various SRFs

The permeability of the water-resistant pillar depends on volumetric stress, water pressure, and the extent of the plastic zone, and changes significantly with the SRF. Figure 7a plots the permeability of the rock pillar at an SRF of 1.10. There is: an excavation-induced enhanced permeability zone, about 1.8 m wide, ahead of the excavated opening, in which the permeability ranges from 0.82×10^{-8} to 9.72×10^{-8} m/s; an approximately constant permeability zone about 5.4 m in width, where the permeability is less than 1.0×10^{-10} m/s; and a second enhanced permeability zone about 1.1 m in width, near the cave, where the permeability ranges from about 3.24×10^{-8} to 9.72×10^{-8} m/s. These three zones correspond approximately to the plastic zone near the excavated opening, the elastic zone, and the plastic zone near the cave, respectively.

The average permeability at a SRF of 1.54 is increased by nearly an order of magnitude (Fig. 7b), which is mainly due to the extension of the plastic zone and decreased volumetric stress. The excavation-induced permeability zone is about 4.5 to 5.0 m wide, where the permeability is between 1.0×10^{-7} and 1.0×10^{-6} m/s. The approximately constant permeability zone is about 1.0 m wide, with a permeability below 5.0×10^{-8} m/s. The enhanced permeability zone near the cave is about 2.0 m wide, with a permeability ranging from 2.0×10^{-7} to 9.0×10^{-7} m/s.

Once the SRF reaches 1.59, numerical non-convergence occurs, which indicates that the pillar loses its stability. The average permeability at a SRF of 1.59 is 5 to 6 times greater than that at a SRF of 1.54. The permeability of the pillar at calculation step N = 6000 is plotted in Fig. 7c; one can see that the three permeability zones have disappeared.

Figure 8 shows the steady seepage field distribution, which indicates that a relatively high average hydraulic pressure gradient of 0.5 MPa/m is intensively distributed in the pillar. The volumetric stress is applied horizontally to the pillar by the hydraulic pressure gradient, which is a more critical force with respect to water-inrush than mining-induced stress.

Criterion for Establishing the Width of the Water-resistant Rock Pillar

Based on the HM-SRM method, the FOS values of the water-resistant pillar can be determined at the various karst water pressures and pillar widths. Figure 9 illustrates how FOS varies with karst water pressure and the pillar width, following the exponential function:

$$FOS = a + b\exp(cW), \tag{13}$$

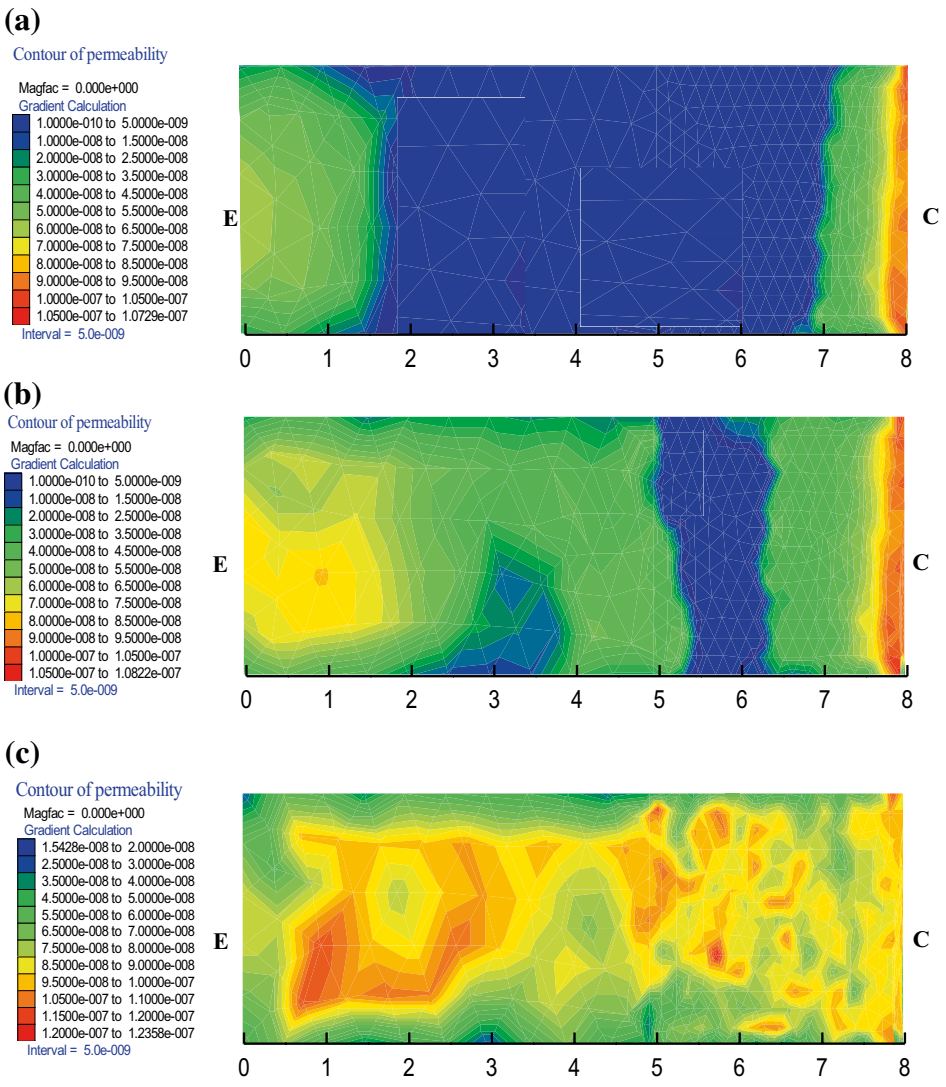

Fig. 7 Permeability distribution of water-resistant rock pillar at SRFs of **a** 1.10, **b** 1.54, and **c** 1.59. The E side is the excavated opening, and the C side is the water-bearing cave

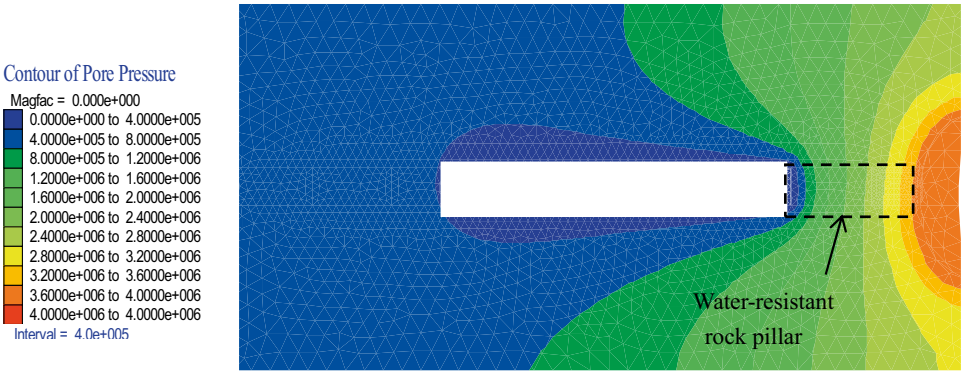

Fig. 8 Steady seepage field distribution

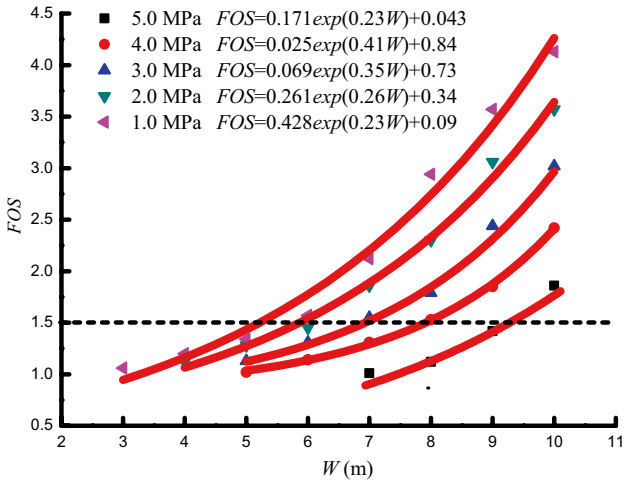

Fig. 9 The FOS versus the width of water-resistant rock pillar W at various water pressures

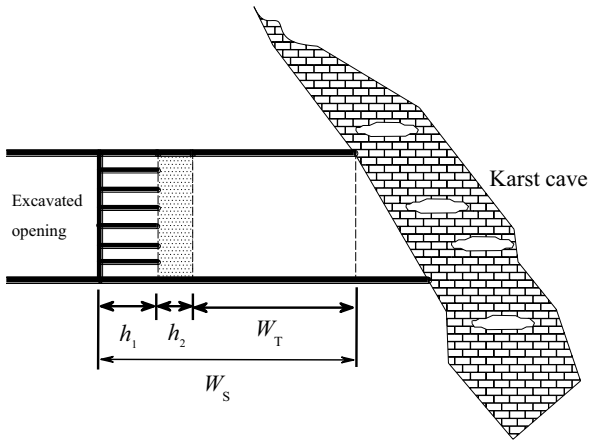

Fig. 10 Schematic diagram of the required width of the water-resistant rock pillar W_S

Table 2 The required width of water-resistant rock at various karst water pressures

Karst water pressure (MPa)	W_T (m)	Blast hole depth h_1 (m)	Blast-disturbance depth h_2 (m)	W_S (m)
1.0	5.18	2.5	1.5	9.18
2.0	5.73	2.5	1.5	9.73
3.0	6.89	2.5	1.5	10.89
4.0	7.98	2.5	1.5	11.98
5.0	9.32	2.5	1.5	13.32

where W is the width of the water-resistant rock pillar, and a, b, and c are fitting coefficients. The fitting functions at various karst water pressures and pillar widths are listed in Fig. 9. Since the discharge and plastic zone both increase sharply when the SRF is above 1.5 (Fig. 6), a FOS of 1.5 is considered to be a critical value in the HM-SRM method to determine a reasonable pillar width. A proposed criterion for the theoretical setting width of the water-resistant rock pillar can be obtained by:

$$W_T \geq W_{1.5}, \tag{14}$$

where W_T is the theoretical width of the water-resistant pillar and $W_{1.5}$ is the width of the pillar at an FOS of 1.5.

The theoretically required width of water-resistant rock, W_T, at various water pressures, is illustrated in Table 2. At karst water pressures of 1.0, 3.0, and 5.0 MPa, the theoretically required width is 5.18, 6.89, and 9.32 m, respectively. This is because that as the karst water pressure increases, the seepage volumetric stress induced by the hydraulic pressure gradient in the pillar increases, which directly enhances lateral thrust along the direction of the excavated opening, so the width of water-resistant rock should be broadened, accordingly.

The drill-blast excavation inevitably disturbs the original strata. Blast-disturbance depth can extend from 0.1 m to as much as 1.5 m into the water-resistant pillar, increasing permeability by two or three orders of magnitude (Tsang 2005). So, in practice, the width of

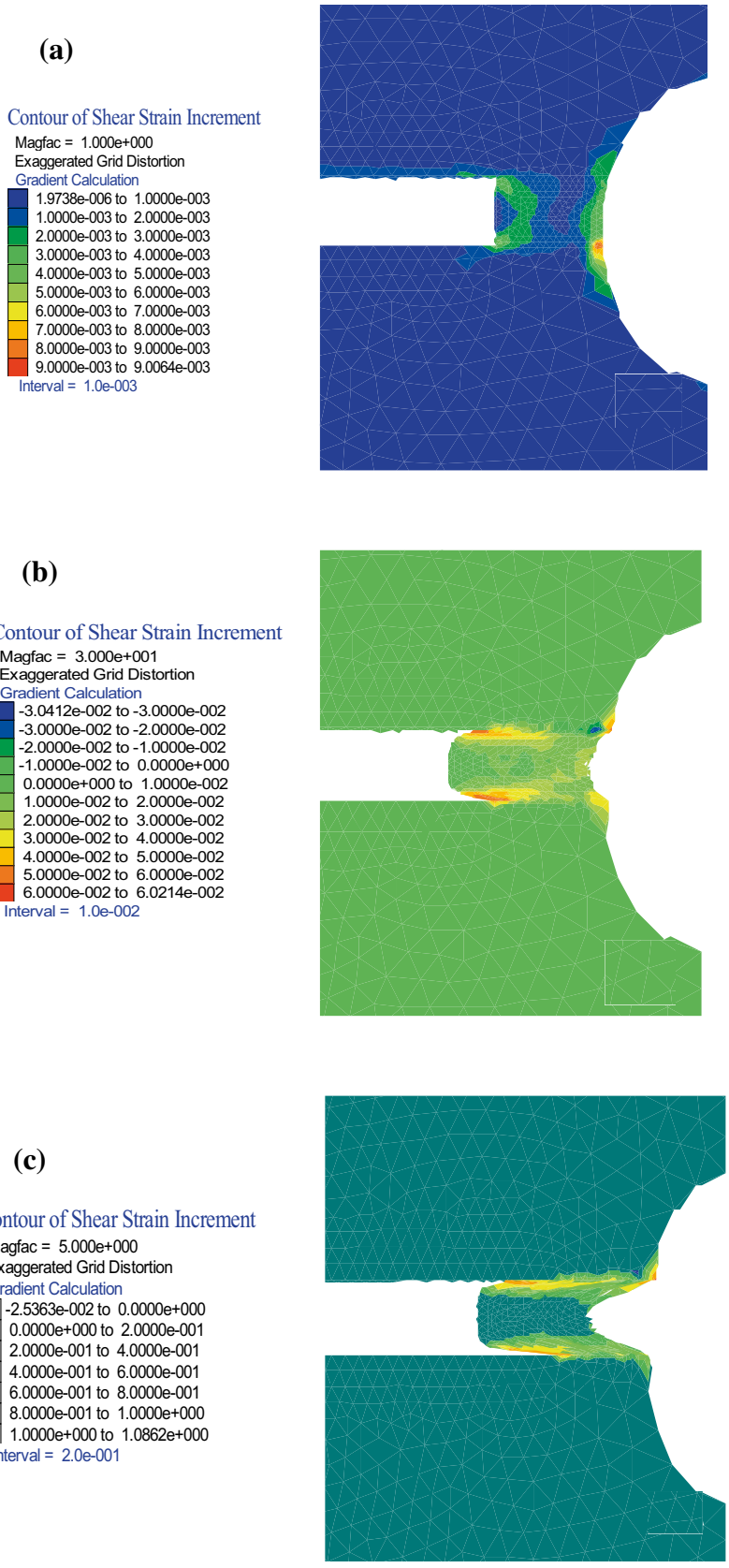

Fig. 11 The instability evolution of the water-resistant rock pillar with a width of 3.0 m at **a** N = 2000 steps, **b** N = 4000 steps, and **c** N = 6000 steps. E side is excavated opening, and C side is water-bearing karst cave

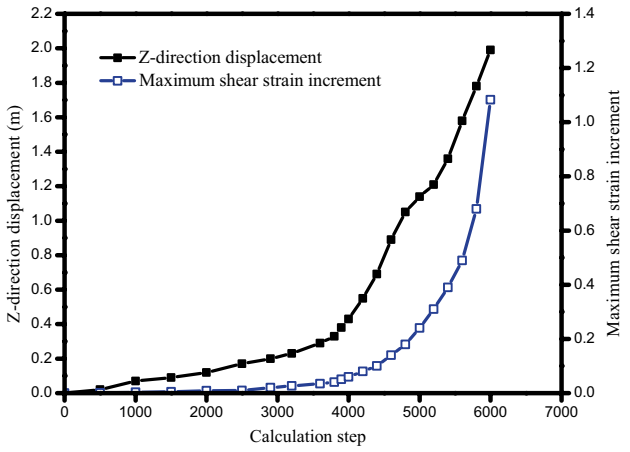

Fig. 12 Z-direction displacement and the maximum shear strain increment of the water-resistant rock pillar versus calculation step

water-resistant pillar, W_S, should be the sum of the theoretically required width (W_T,), the blast hole depth h_1, and the blast-disturbance depth h_2, as shown in Fig. 10.

$$W_S = W_T + h_1 + h_2. \quad (15)$$

The required width of the water-resistant pillar calculated from Eq. (15) at various water pressures is listed in Table 2, in which h_1 and h_2 were set to 2.5 and 1.5 m, respectively, according to practice in the Qiyi coal mine. Table 2 indicates that a reasonable pillar width should be about 10–14 m, for karst water pressures of about 1.0 to 5.0 MPa, given the geological conditions of the Qiyi coal mine.

Evolution of Rock Pillar Instability

The investigation of the "4·16" accident suggested that a water-bearing cave with a volume of 20 m×6 m×20 m was about 3 m from the heading face, i.e. the width of the water-resistant rock pillar was about 3 m. Making matters worse, the cave was very likely hydrologically connected to the surface, so that the water pressure in the cave was about 4.0 MPa. Based on Table 2, the rock pillar should have been 11 to 12 m wide.

Figure 11a–c show how the instability evolved once the pillar width was set at 3.0 m. As calculation steps, N, increase, the shear strain increment, which is an indication of the shear fail faces, was highly concentrated on the interfaces between the water-resistant pillar, the roof, and the floor. The calculation result did not converge to a steady value, the model failed to equilibrate, and the maximum shear strain increment rapidly increased (Fig. 12). The calculated Z-direction displacement of the excavated opening increased exponentially from 0.12 m at $N=2000$, to 0.38 m at $N=4000$, up to nearly 2.0 m when $N=6000$. Both the maximum shear strain increment and Z-direction displacement of the water-resistant pillar increased at great rates, and failed to converge to a steady value, which indicates that the 3.0 m wide water-resistant pillar was unstable.

Conclusions

A HM-SRM method was proposed to evaluate the stability of water-resistant rock pillars. The FOS of the pillar was established, and a new criterion for a reasonable pillar width in engineering practice was developed.

Water inrush was linked with the non-convergence of the mechanical calculations, and the seepage characteristics closely correlated with the stress state and plastic failure zone in the proposed hydro-mechanical coupling model.

As the SRF increases, the effective width of the water-resistant pillar narrows and the water-resistant pillar becomes more permeable, enhancing the probability of water inrush.

In engineering practice, the width of water-resistant rock pillar should at least equal the sum of the theoretical required width of water-resistant rock (based on a FOS of 1.5), plus the blast hole depth and the blast-disturbance depth.

The "4·16" accident in the Qiyi coal mine occurred because the roadway was only 3.0 m from the water-bearing cave. Considering the blast hole depth and the likely blast disturbance to the intervening rock, a water-resistant pillar at least 11 m wide was needed to safely hold back a karst water pressure of nearly 4.0 MPa.

Acknowledgements The authors thank the National Natural Science Foundation of China (Grants 51274097, 51434006, 51304057), the Natural Science Foundation of Hunan province (2015JJ2067), and the Open Projects of State Key Laboratory of Coal Resources and Safe Mining, CUMT (SKLCRSM16KF12) for their financial support.

References

Cheng YM, Lansivaara T, Wei WB (2007) Two-dimensional slope stability analysis by limit equilibrium and strength reduction methods. Comput Geotech 34:137–150

Cundall PA (2001) FLAC manual: a computer program for fast lagrangian analysis of continua. 1st revision. Itasca Consulting Group Inc, Minneapolis

Dai S, Ren D, Tang Y, Yue M, Hao L (2005) Concentration and distribution of elements in Late Permian coals from western Guizhou Province, China. Int J Coal Geol 61(1):119–137

David C, Menendez B, Zhu W, Wong TF (2001) Mechanical compaction, microstructures and permeability evolution in sandstones. Phys Chem Earth (A) 26: 45–51

Dawson EM, Roth WH, Drescher A (1999) Slope stability analysis by strength reduction. Geotechnique 49(6):835–840

Griffiths DV, Lane PA (1999) Slope stability analysis by finite elements. Geotechnique 49(3):387–403

Guo H, Adhikary D, Craig M (2009) Simulation of mine water inflow and gas emission during longwall mining. Rock Mech Rock Eng 42(1):25–51

He KQ, YU YJ, Fei W (2011) Overview of karst geo-environments and karst water resources in north and south China. Environ Earth Sci 64:1865–1873

He KQ, Wang RL, Jiang WF (2012) Groundwater inrush channel detection and curtain grouting of the Gaoyang iron ore mine, China. Mine Water Environ 31(4):297–306

Itasca Consulting Group Inc (2002) Fast Lagrangian analysis of continua in 3-Dimensions. Itasca Consulting Group, Minnesota

Jing L (2003) A review of techniques, advances and outstanding issues in numerical modelling for rock mechanics and rock engineering. Int J Rock Mech Min 40(3):283–353

Li SP, Li YS, Li Y, Wu ZY, Zhou G (1994) Permeability-strain equations corresponding to the complete stress-strain path of Yinzhuang sandstone. Int J Rock Mech Min Sci Geomech Abstr 31(4):383–391

Li LH, Yang TH, Liang ZZ, Zhu WC, Tang CA (2011) Numerical investigation of groundwater outbursts near faults in underground coal mines. Int J Coal Geol 85(3):276–288

Lin H, Cao P, Li JT, Jiang XL, He ZM (2010) Deformation stability of three-dimensional slope based on Hoek-Brown criterion. Rock Soil Mech 31:3656–3660 **(Chinese)**

Louis C (1974) Rock hydraulics. In: Muller L (ed) Rock mechanics. Springer, New York, pp 300–387

Lu Y, Wang L (2015) Numerical simulation of mining-induced fracture evolution and water flow in coal seam floor above a confined aquifer. Comput Geotech 67:157–171

Matsui T, San KC (1992) Finite element slope stability analysis by shear strength reduction technique. Soils Found 32(1):59–70

Miao XX, Wang A, Sun YJ (2009) Research on theory of mining with water resources protection and its application to arid and semi-arid mining region. Chin J Rock Mech Eng 28(2):217–227 **(In Chinese)**

Miao XX, Cui XM, Wang JA, Xu JL (2011) The height of fractured water-conducting zone in undermined rock strata. Eng Geol 20(1):32–39

Shi L, Singh RN (2001) Study of mine water inrush from floor strata through faults. Mine Water Environ 20(3):140–147

Sun W, Wu Q, Dong D, Jiao J (2012) Avoiding coal–water conflicts during the development of China's large coal-producing regions. Mine Water Environ 31(1):74–78

Tang CA (1997) Numerical simulation on progressive failure leading to collapse and associated seismicity. Int J Rock Mech Min Sci 34(2):249–261

Tsang CF, Bernier F, Davies C (2005) Geohydromechanical processes in the excavation damaged zone in crystalline rock, rock salt, and indurated and plastic clays-in the context of radioactive waste disposal. Int J Rock Mech Min 42(1):109–125

Wang JA, Park H (2003) Coal mining above a confined aquifer. Int J Rock Mech Min 40(4):537–551

Wang CS, Bai HB, Liu SC (2010) Mine water issues in China. Mine Water and Innovative Thinking, Proc, IMWA 2010 Symp, Sydney, NS, Canada, pp 445–448

Wu Q, Wang M (2006) Characterization of water bursting and discharge into underground mines with multi-layered groundwater flow systems in the north China coal basin. Hydrogeol J 14(6):882–893

Wu Q, Wang M, Wu X (2004) Investigations of groundwater bursting into coal mine seam floors from fault zones. Int J Rock Mech Min Sci 41(4):557–571

Xiao GC, Irvin RA, Farmer IW (1991) Water inflows into longwall workings in the proximity of aquifer rocks. Min Eng 151(358):9–13

Yang XL, Huang F (2009) Stability analysis of shallow tunnels subjected to seepage with strength reduction theory. J Cent South Univ 16:1001–1005

Yang TH, Tham LG, Tang CA, Liang ZZ, Tsui Y (2004) Influence of heterogeneity of mechanical properties on hydraulic fracturing in permeable rocks. Rock Mech Rock Eng 37(4):251–275

Yang TH, Liu J, Zhu WC, Elsworth D, Tham LG, Tang CA (2007) A coupled flow-stress-damage model for groundwater outbursts from an underlying aquifer into mining excavations. Int J Rock Mech Min 44(1):87–97

Yu L, Liu J (2015) Stability of interbed for salt cavern gas storage in solution mining considering cusp displacement catastrophe theory. Petrol 1:82–90

Zhang JC (2005) Investigations of water inrushes from aquifers under coal seams. Int J Rock Mech Min Sci 42:350–360

Zhang HQ, He YN, Tang CA., Ahmad B, Han LJ (2009) Application of an improved flow-stress- damage model to the criticality assessment of water inrush in a mine: a case study. Rock Mech Rock Eng 42:911–930

Zhao YL, Wu QH, Wang WJ, Wan W, Zhao FJ (2010) Strength reduction method to study stability of goaf overlapping roof based on catastrophe theory. Chin J Rock Mech Eng 29(7):1424–1434 **(In Chinese)**

Zhao YL, Tang JZ, Chen Y, Zhang LY. Wang WJ, Wan W, Liao JP (2017) Hydromechanical coupling tests for mechanical and permeability characteristics of fractured limestone in complete stress–strain process. Environ Earth Sci 76:1–18

Zhu B, Wu Q, Yang J, Cui T (2013) Study of pore pressure change during mining and its application on water inrush prevention: a numerical simulation case in Zhaogezhuang coal mine, China. Environ Earth Sci 71(50):2115–2132

Zienkiewicz OC, Humpheson C, Lewis RW (1975) Associated and non-associated visco-plasticity and plasticity in soil mechanics. Geotechnique 25(4):671–689